




# Dynamics of sleep oscillations is coupled to brain temperature on multiple scales

Márton Csernai<sup>1</sup>, Sándor Borbély<sup>1,2</sup>, Kinga Kocsis<sup>1,3,4</sup> , Dávid Burka<sup>1,9</sup>, Zoltán Fekete<sup>5,6</sup> ,  
Veronika Balogh<sup>1</sup>, Szabolcs Káli<sup>7</sup>, Zsuzsa Emri<sup>8</sup> and Péter Barthó<sup>1</sup> 

<sup>1</sup>Institute of Cognitive Neuroscience and Psychology, Research Centre for Natural Sciences, Hungarian Academy of Sciences, Budapest, Hungary

<sup>2</sup>Department of Physiology and Neurobiology, Eötvös Loránd University, Budapest, Hungary

<sup>3</sup>Roska Tamás Doctoral School of Sciences and Technology, Faculty of Information Technology and Bionics, Pázmány Péter Catholic University, Budapest, Hungary

<sup>4</sup>Neuronal Network and Behavior Research Group, RCNS, Hungarian Academy of Sciences, Budapest, Hungary

<sup>5</sup>Research Group for Implantable Microsystems, Faculty of Information Technology and Bionics, Pázmány Péter Catholic University, Budapest, Hungary

<sup>6</sup>Institute of Technical Physics and Material Science, Centre for Energy Research, Hungarian Academy of Sciences, Budapest, Hungary

<sup>7</sup>Institute of Experimental Medicine, Hungarian Academy of Sciences, Budapest, Hungary

<sup>8</sup>Eszterházy Károly University, Eger, Hungary

<sup>9</sup>Corvinus University of Budapest, Budapest, Hungary,

Edited by: Ole Paulsen & Diego Contreras

## Key points

- Sleep spindle frequency positively, duration negatively correlates with brain temperature.
- Local heating of the thalamus produces similar effects in the heated area.
- Thalamic network model corroborates temperature dependence of sleep spindle frequency.
- Brain temperature shows spontaneous microfluctuations during both anesthesia and natural sleep.
- Larger fluctuations are associated with epochs of REM sleep.
- Smaller fluctuations correspond to the alteration of spindling and delta epochs of infra-slow oscillation.

**Abstract** Every form of neural activity depends on temperature, yet its relationship to brain rhythms is poorly understood. In this work we examined how sleep spindles are influenced by changing brain temperatures and how brain temperature is influenced by sleep oscillations. We employed a novel thermoelectrode designed for measuring temperature while recording neural activity. We found that spindle frequency is positively correlated and duration negatively correlated with brain temperature. Local heating of the thalamus replicated the temperature dependence of spindle parameters in the heated area only, suggesting biophysical rather than global modulatory mechanisms, a finding also supported by a thalamic network model. Finally,

**Marton Csernai** is a postdoctoral researcher with a background in electrical engineering and computer science. His primary research focuses on the network effects of sleep processes, especially how cell ensembles behave during sleep spindles.



M. Csernai, S. Borbély and K. Kocsis contributed equally to this work.

we show that switches between oscillatory states also influence brain temperature on a shorter and smaller scale. Epochs of paradoxical sleep as well as the infra-slow oscillation were associated with brain temperature fluctuations below 0.2°C. Our results highlight that brain temperature is massively intertwined with sleep oscillations on various time scales.

(Received 11 January 2019; accepted after revision 11 June 2019; first published online 13 June 2019)

**Corresponding author** P. Barthó: Institute of Cognitive Neuroscience and Psychology, Research Centre for Natural Sciences, Hungarian Academy of Sciences, Budapest, Hungary, 1117 Magyar Tudósok Krt. 2.

Email bartho.peter@ttk.mta.hu

## Introduction

Sleep is essential for our everyday functioning, as well as for memory consolidation. Several factors influence sleep, temperature being amongst the most important. Sleep quality and propensity are highly dependent on thermal conditions; sleep regulation is tightly coupled to thermoregulation. On the other hand, there are multiple sleep-related changes in body and brain temperature independent of the circadian rhythm.

Studies in mammalian species have shown that there are multiple changes in body and brain temperature during a single sleep session. Non-rapid eye movement (non-REM) sleep is associated with decreased brain and body temperature, while during REM sleep, despite the reduced somatic thermal regulation, brain temperature increases (Kawamura & Sawyer, 1965; Baker & Hayward, 1967; Satoh, 1968; Kovalzon, 1973; Alföldi *et al.* 1990; Lyamin *et al.* 2018).

Besides these short-term changes, core body temperature can vary across individuals (Sund-Levander *et al.* 2002) with changes in ambient temperature (Alföldi *et al.* 1990), in pathological conditions such as hypo- or hyperthyroidism (Fregly *et al.* 1961), during the oestrus cycle (Driver *et al.* 1996), or as a result of medical or recreational drug use (Kiyatkin, 2010). Furthermore, though brain temperature is widely recognized as a strictly regulated homeostatic parameter, it can change as much as 3°C across different arousal states and during sensory stimulation as shown across many avian and mammalian species (Delgado & Hanai, 1966; McElligott & Melzack, 1967; Kovalzon, 1973; Kiyatkin *et al.* 2002; Mitchell *et al.* 2006; Trübel *et al.* 2006), as well as in clinical human studies (Mellergård, 1995; Rossi, 2001).

The tight relationship between core body temperature and sleep stages was also verified by directly manipulating one or other of them. Changes in body temperature have the potential to entrain brain state fluctuations (Whitten *et al.* 2009); also baseline temperature influences particular brain oscillations. A brain temperature change of 1°C is sufficient to shift EEG frequencies above 10 Hz by 1 Hz (Deboer & Tobler, 1995). Lowering body temperature results in a decreasing EEG amplitude (Massopust *et al.* 1965; Michenfelder & Milde, 1991) and a shift towards lower frequencies (Deboer & Tobler,

1995). Direct cooling of the neocortex can switch slow-wave to desynchronized activity patterns (Sheroziya & Timofeev, 2015). Temperature-dependent changes in brain oscillations which reflect the activity of synchronized neural populations, point towards deeper consequences in network function.

Amongst thalamocortical oscillations, sleep spindles (7–15 Hz, 1–3 s) have been the subject of many studies on sleep quality, memory encoding and mental health. These transient oscillations play a critical role in learning (Fogel *et al.* 2007; Morin *et al.* 2008) and mark sleep fragility (Lecci *et al.* 2017); at the same time they are very susceptible to thermal changes of the mammalian body. Thus, it is essential to study how spindle dynamics are affected by body and brain temperature variations. It has been shown that the frequency of sleep spindle oscillations co-varies with physiological body temperature changes recurring across the menstrual cycle. Spindle activity also shows a circadian modulation with a peak density at habitual sleep onset, time locked to the maximal decrease in core temperature (Dijk & Czeisler, 1995).

Given the large natural variability in brain temperature across individuals and conditions, it is extremely important to shed light on its relationship with neural oscillations. Medications and external thermal conditions both alter brain temperature and should therefore be considered as a factor in medical procedures. On the other hand, brain temperature should be taken into consideration when conducting *in vivo* neurophysiological experiments, as well as for *in silico* network models, in order to mimic natural state changes.

In this study we seek to elucidate the biophysical and network mechanisms underlying the relationship between sleep oscillations and brain temperature. We investigate the changes in these oscillations, especially sleep spindles, while manipulating core as well as brain temperature, and finally we show how oscillations relate to brain temperature without external manipulation.

## Methods

### Ethical considerations

Experiments were carried out in accordance with the Hungarian Act of Animal Care and Experimentation

(1998, XXVIII) and with the directive 2010/63/EU of the European Parliament and of the Council of 22 September 2010 on the protection of animals used for scientific purposes. The experimental protocol was approved by the regional ethical committee (licence number PEI/001/2290-11/2015 for our *in vivo* experiments). Efforts were made to minimize the number of animals used.

Mice were kept under a 12 h:12 h light–dark cycle (lights on at 07:00 h) in a temperature-controlled room at  $22 \pm 2^\circ\text{C}$ . Standard food pellets and tap water were available *ad libitum*.

### Electrophysiological and temperature recordings

**Acute experiments.** Our experiments were performed on 13 male C57BL/6 mice (Toxicop, Budapest, Hungary) weighing between 18 and 30 g at the time of the surgery. For general surgical procedures see Barthó *et al.* (2004). Briefly, the animals were anaesthetized with urethane ( $1.2 \text{ g kg}^{-1}$ ; i.p.), then placed in a stereotaxic instrument (RWD Life Science, Shenzhen, China). Small ( $<0.5 \text{ mm}$ ) craniotomies were made over the target brain areas, and electrodes were lowered into the brain at a speed below  $0.2 \text{ mm s}^{-1}$ . After electrode insertion, we waited 30 min before recording.

To record local field potential (LFP) activity, NeuroNexus (Ann Arbor, MI, USA) silicon probes were inserted into the brain. Linear 16-channel silicon probes were inserted into the left primary somatosensory cortex (Br. AP 0.0, L +3.5, in  $18^\circ$  at  $1600 \mu\text{m}$  depth), and in the left ventral posteromedial nucleus (VPM) of thalamus (Br. AP  $-1.6$ , L +2.3, in  $18^\circ$  at  $3700 \mu\text{m}$  depth). Our custom-designed thermoelectrode, featuring four electrophysiological recording sites and a platinum temperature sensor, was inserted also into the left VPM (Br. AP  $-1.6$ , L +1.6, in  $0^\circ$  at  $3600 \mu\text{m}$  depth). In some experiments the linear 16-channel probe was inserted into the right primary somatosensory cortex (Br. AP 0.0, L  $-3.5$ , in  $18^\circ$  at  $1600 \mu\text{m}$  depth) or to the right VPM (Br. AP  $-1.6$ , L  $-2.3$ , in  $18^\circ$  at  $3700 \mu\text{m}$  depth). In this case there was no recording from the left cortical area. An additional screw electrode implanted over the cerebellum served as a reference. Co-ordinates are based on the stereotaxic atlas of Paxinos & Watson (1986). Using a unipolar  $V_1$  ECG lead, heart rate and electrocardiogram were simultaneously recorded with LFP. Rectal temperature was measured by a TH-5 Thermalert Monitoring Thermometer (Physitemp, Clifton, NJ, USA).

Recordings were made with Intan RHD2132 16-channel amplifiers, connected to an RHD-2000 Evaluation Board (Intan Technologies, Los Angeles, CA, USA). Brain temperature was measured by calibrating and measuring the resistance of the platinum filament in the thermoelectrode (see details in Fekete *et al.* 2017) by a Keithley 6221 precision current generator and a Keithley 2000MM

multimeter (Keithley Instruments Inc., Solon, OH, USA). Rectal temperature signals were simultaneously recorded by using the analog inputs of the Intan RHD-2000 system. All signals were sampled at 20 kHz, except for brain temperature which was sampled at 5 Hz and synchronized to the other signals through the analog input of the Intan system.

**Chronic experiments.** These experiments were carried out on five male C57BL/6 mice (Toxicop, Budapest, Hungary) weighing between 27 and 35 g at the time of the surgery. For initial surgery, animals were anaesthetized with ketamine/xylazine (ketamine:  $100 \text{ mg kg}^{-1}$ ; xylazine:  $4 \text{ mg kg}^{-1}$ ; i.p.), then placed in a stereotaxic instrument (RWD Life Science). During surgery, the depth of anaesthesia was regularly assessed by the limb-withdrawal or corneal reflex, and an additional dose of anaesthetic was administered, if necessary.

To record LFP and multiunit activity (MUA), bundles of 25 and  $50 \mu\text{m}$  tungsten stereotrodes (California Fine Wire, Grover Beach, CA, USA) were used. Electrodes were placed in the left and right S1 (Br. AP 0.0, L  $\pm 3.5$ , at  $1000 \mu\text{m}$  depth), the ventral posteromedial thalamus (VPM) (Br. AP  $-1.6$ , L +2.5, in  $18^\circ$  at  $3700 \mu\text{m}$  depth), as well as in the hippocampus (Br. AP  $-1.6$ , L  $-1.5$ , in  $0^\circ$  at  $2200 \mu\text{m}$  depth). To record temperature, a  $0.3 \text{ mm}$  diameter Semitec thermistor (223F $\mu$ 3122-07U015; Mouser Electronics, Mansfield, TX, USA) was also inserted to left VPM (Br. AP  $-1.6$ , L +1.5, in  $0^\circ$  at  $3600 \mu\text{m}$  depth). An EMG electrode was placed in the neck musculature. Co-ordinates are based on the stereotaxic atlas of Paxinos and Watson (1986). Electrodes were connected to a Neuralynx EIB-16 electrode interface board (Neuralynx, Dublin, Ireland). Core body temperature was measured intraperitoneally by Semitec thermistors (223F $\mu$ 3122-07U015, Mouser Electronics).

During the recovery period (10 days), animals were given analgesic medication in their drinking water (ibuprofen) and monitored daily for signs of pain or inflammation. After recovery, signals were recorded continuously for 6–8 h per day during wakefulness and natural sleep with the same system as acute experiments. The behaviour of animals was also recorded using a commercially available CCD camera.

### Accuracy of brain temperature recording

In the thermoprobe recordings, the accuracy of absolute temperature was below  $0.14^\circ\text{C}$  (Fekete *et al.* 2017). The sensitivity of the device to relative changes in temperature, which is required to measure microfluctuations, however, is magnitudes higher. At  $33^\circ\text{C}$  the resistance and temperature coefficient of the integrated platinum temperature filament is  $R_0 = 335.81 \pm 18.22 \Omega$  and  $\alpha = 1721 \pm 99 \text{ p.p.m. K}^{-1}$ . This means that an approximately  $0.002 \Omega$  change in resistance corresponds

to a temperature change of  $0.01^{\circ}\text{C}$ . The resolution of the Keithley 2000MM unit is  $0.001\ \Omega$  in a range of  $1\ \text{k}\Omega$ . Based on these data, it is accurate enough to evaluate variations in temperature as small as  $0.01^{\circ}\text{C}$ . In the case of the Semitec thermistor, there is a non-linear relationship between resistance and temperature governed by the so-called thermistor equation. The B value of the thermistor is 3454 and its rated zero-power resistance is  $14,015\ \Omega$  at  $37^{\circ}\text{C}$ . If the temperature changes from e.g.  $37$  to  $38^{\circ}\text{C}$ , it corresponds to a decrease in resistance by approximately  $500\ \Omega$ . To simplify this case, considering the relationship to be linear in this range, a  $0.01\ \text{K}$  change induces a  $5\ \Omega$  decrease, which can be accurately and easily measured by the setup.

### Histology

Following the recordings, under deep anaesthesia mice were transcardially perfused with  $0.9\%$  saline, followed by fixative containing  $4\%$  paraformaldehyde and  $0.1\ \text{M}$  phosphate buffer (PB). After perfusion brains were sliced to  $50\ \mu\text{m}$ -thick coronal sections with a vibratome. Before each acute experiment, silicon probes were dipped in DiI solution for verification of recording sites. After further PB washes, sections were mounted temporarily in PB and imaged using epifluorescent microscopy (Leica).

The electrode tracks of the thermo probes were reconstructed from counterstained glial fibrillary acidic protein (GFAP). GFAP staining were used to visualize the lesion made by the thermo probes and to check whether heating caused necrosis in the adjacent tissue. After imaging silicon probe tracks, the same sections were subjected to immunofluorescence staining according to the following protocol. After further PB washes, sections were freeze-thawed above liquid  $\text{N}_2$  in  $0.1\ \text{M}$  PB containing  $30\%$  sucrose. Endogenous peroxidase activity was blocked with  $1\% \text{H}_2\text{O}_2$ , then non-specific staining was suppressed with  $2\%$  normal horse serum (Vector Laboratories, Burlingame, CA, USA) in  $0.1\ \text{M}$  PB. Monoclonal mouse antibodies were used against GFAP (1:2000, EMD Millipore, Merck, Darmstadt, Germany, clone GA5) for  $24\ \text{h}$  at  $4^{\circ}\text{C}$ . Immunopositive elements were visualized using biotinylated anti-mouse immunoglobulin G (1:250, Vector Laboratories) as a secondary antiserum followed by avidin-biotinylated horseradish peroxidase complex (ABC; 1:250, Vector Laboratories). The immunoperoxidase reaction was developed using  $3,3'$ -diaminobenzidine tetrahydrochloride (DAB; Sigma, St Louis, MO, USA) dissolved in Tris buffer (pH 7.6) as a chromogen. After washing in Tris buffer and PB, sections were mounted, dehydrated for light microscopy ( $2 \times 10\ \text{min}$  in xylene) and coverslipped with DePex (Serva Electrophoresis GmbH, Heidelberg, Germany). We found no necrosis in any of the animals.

### Local heating of brain tissue

The platinum filament in the thermoelectrode can be used to heat up neighbouring brain tissue by increasing the current in the four-wire resistance measurement setup. The technical and histological details are described in Fekete *et al.* (2017). Briefly, we employed  $2\ \text{min}$  of measurement current ( $1\ \text{mA}$ ) and  $2\ \text{min}$  of heating current ( $4\text{--}8\ \text{mA}$ ) in a cyclic pattern. An exponential was fitted on the measured temperature values from  $400\ \text{ms}$  after the offset of the heating current in each cycle and temperature during heating was estimated by the intersection of the exponential and the offset time of the heating pulse.

Distance dependence of heating was calculated by locally heating the brain tissue with the thermoprobe at  $4, 6$  and  $8\ \text{mA}$  currents for  $50\ \text{s}$ , while measuring the elicited temperature change with a Semitec thermistor inserted at  $0.5, 1$  and  $3\ \text{mm}$  distances, consecutively. Only the temperature value by the end of the heating was considered.

### Data analysis

**Electrophysiology.** Raw LFP channels were band pass filtered between  $0.4$  and  $7\ \text{kHz}$ , and multiunits were detected with an absolute threshold. The units were combined from multiple channels, downsampled to  $1\ \text{kHz}$  and smoothed with a  $10\ \text{ms}$  moving average filter. Sigma power was determined by filtering the preprocessed multiunit activity (MUA) between  $6$  and  $18\ \text{Hz}$ . In the case of the analysis of infra-slow oscillations we used sigma power from the best recording sites. Theta power was calculated by first downsampling hippocampal LFP to  $1\ \text{kHz}$ , and then taking the ratio of the theta ( $6\text{--}10\ \text{Hz}$ ) and delta ( $0.5\text{--}4\ \text{Hz}$ ) bands. Heart rate was smoothed with a  $10\ \text{s}$  moving average window. Sigma band, MUA and EMG activity were normalized to their means.

**Temperature.** In general, all temperature data were downsampled to  $1\ \text{kHz}$  and smoothed with a  $100\ \text{ms}$  window, except for brain temperature in the acute experiments, in which case we simply used the recorded samples that were synchronized to the other signals. In the case of the analysis of infra-slow oscillations, all respective signals were smoothed with a  $10\ \text{s}$  window and then downsampled to  $10\ \text{Hz}$ , while brain temperatures of the acute experiments were interpolated to  $10\ \text{Hz}$ . Large fluctuations were marked manually based on visual features of joint brain temperature and theta power increase motifs. Small fluctuation epochs were selected between the large elevations. Small fluctuation cycle peaks and troughs were detected automatically by the findpeaks MATLAB function (MATLAB software, MathWorks, Natick, MA, USA), and we manually validated these detected peaks in each epoch.

**Spindle detection and frequency calculation.** Spindles were detected semi-automatically from the multiunit activity. MUA was downsampled to 1 kHz, represented as a vector of 1 s and 0 s, smoothed with an 11 s long rectangular filter, and further filtered between 8 and 20 Hz. Automatic detection threshold was set to 1 SD, with a minimum length of 300 ms. Since simple thresholding sometimes spuriously detects desynchronized activity, these events were manually removed. Also, since our analysis is sensitive to missed cycles, spindles with a break in rhythmicity (gap >150 ms) were omitted. Frequency of the spindle was calculated from the average of the time difference between automatically detected cycle peaks (Fig. 1B). The temperature of the spindle is defined as the temperature at the start of the respective spindle. Spindle prevalences were calculated in 2 min bins.

**Sleep scoring.** Wake epochs were defined by the normalized EMG activity exceeding a set threshold for  $\geq 16$  s, while between 0.5 and 16 s duration they were considered microarousals. Desynchronized multiunit activity was often contaminated by muscle artifacts and therefore was not included as a criterion. REM epochs were detected by the threshold (2–2.5, depending on the quality of hippocampal LFP) crossing of hippocampal theta/delta ratio, as well as EMG activity below the threshold. We did not observe complete muscle atonia during REM, thus the onsets of REM epochs were marked solely by the theta/delta threshold crossing.

## Model

For the purpose of this study we adapted the network model of thalamocortical (TC) and thalamic reticular (nRT) cells, constructed by Destexhe *et al.* (1994, 1996) in the NEURON modelling environment. Single compartment TC and nRT cell membrane potential was governed by the following equations:

$$C_m \dot{V}_{TC} = -g_L (V_{TC} - E_L) - I_{KL} - I_T - I_h - I_{Na} - I_K - I_{GABA_A} \quad (1)$$

$$C_m \dot{V}_{nRT} = -g_L (V_{nRT} - E_L) - I_{T2} - I_{CAN} - I_{AHP} - I_{Na} - I_K - I_{AMPA} \quad (2)$$

where  $V_{TC}$  and  $V_{nRT}$  are the membrane potentials of TC and nRT cells respectively, the dots on the left-hand-side denote time derivatives, while  $C_m = 1 \mu\text{F cm}^{-2}$  is the specific capacitance of the membrane. The first term on the right-hand-side of each equation is the leak current, in which  $g_L$  is the leak conductance and  $E_L$  is the reversal potential of the leakage. In the case of the TC cells the leak potassium current ( $I_{KL}$ ) is implemented

separately from the other leakage.  $I_T$  and  $I_{T2}$  are low threshold calcium currents, where the second is a slower version used in the nRT cells.  $I_h$  is the hyperpolarization activated cation current of the TC cells. The nRT cells also include a calcium activated non-selective cation current ( $I_{CAN}$ ) and a slow calcium dependent potassium current ( $I_{AHP}$ ) (Destexhe *et al.* 1994).  $I_{Na}$  and  $I_K$  are sodium and potassium currents that generate action potentials based on the Hodgkin–Huxley model.  $I_{GABA_A}$  is the current of the GABA<sub>A</sub> receptors that appear in the synapses from nRT to TC cells, and  $I_{AMPA}$  is the current of the AMPA receptors in the TC to nRT synapses.

TC cells activated nRT cells via AMPA receptors while nRT cells inhibited TC cells via GABA<sub>A</sub> receptors. We disregarded GABA<sub>B</sub> receptors since their blockade hardly altered spindle oscillations experimentally (Krosigk *et al.* 1993; Bal *et al.* 1995).

## Temperature dependence of the model

Non-synaptic (voltage-gated and calcium-dependent) currents of the original Destexhe models, which were described by a Hodgkin–Huxley-type formalism, already had built-in temperature dependencies. Specifically, the transition rates for channel gating variables were modified by the following multiplier:

$$\varphi_x = Q_{10}^{\frac{T-T_{\text{exp}}}{10^\circ\text{C}}} \quad (3)$$

where  $T$  is the actual temperature and  $T_{\text{exp}}$  is the experimental temperature at which the transition rates and the temperature coefficients ( $Q_{10}$ ) were measured.

Synaptic currents were based on the models constructed by Destexhe *et al.* (1996), supplemented with temperature dependency. All synaptic currents in the model can be described by the following equations:

$$I_{\text{syn}} = \bar{g}_{\text{syn}} r (V - E_{\text{syn}}) \quad (4)$$

$$\frac{dr}{dt} = \alpha [C] (1 - r) - \beta r \quad (5)$$

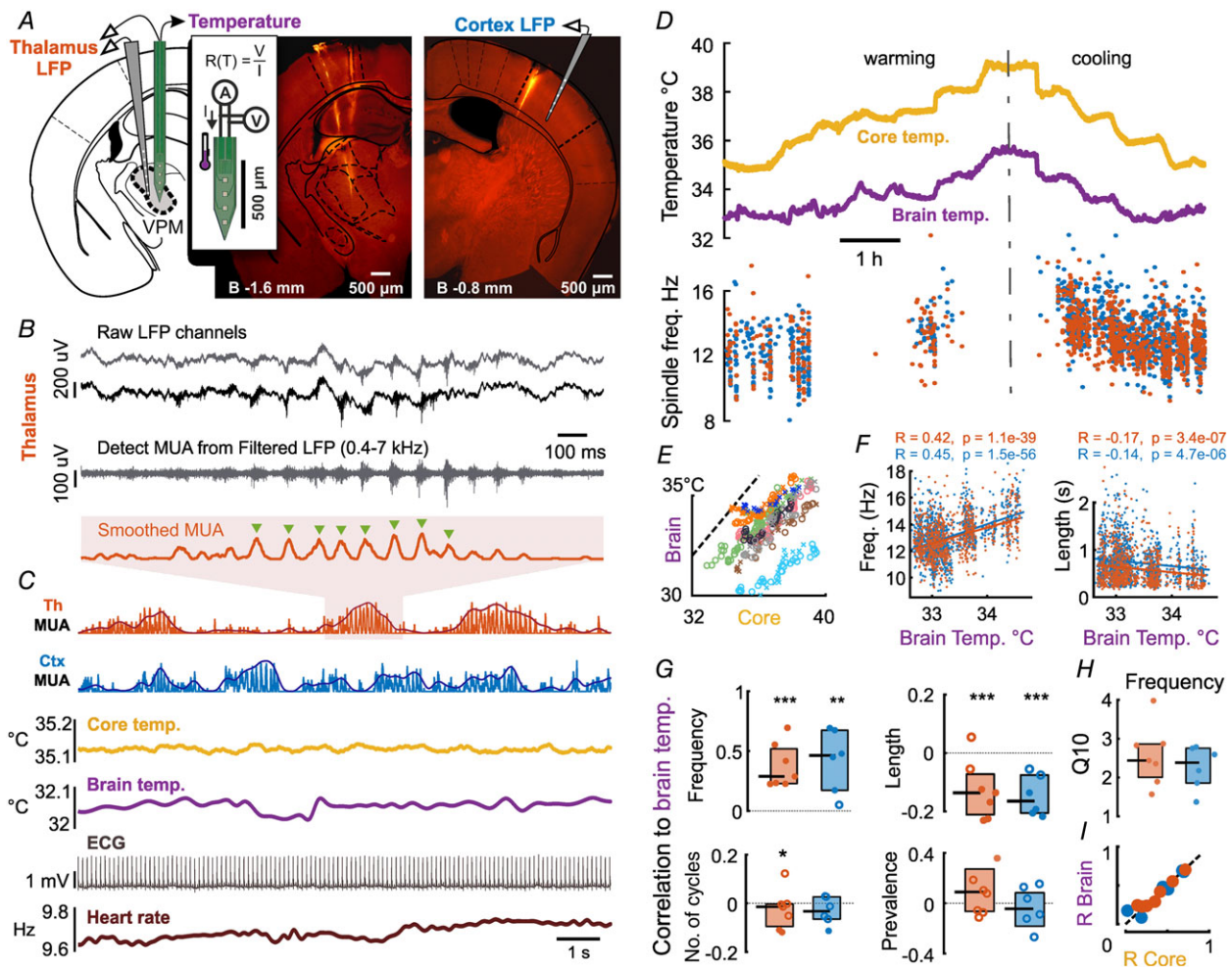
where ‘syn’ can be either for AMPA or GABA<sub>A</sub>, and  $I_{\text{syn}}$  is the synaptic current,  $\bar{g}_{\text{syn}}$  is the maximal conductance and  $E_{\text{syn}}$  is the reversal potential. The fraction of open channels is denoted by  $r$  and  $[C]$  is the concentration of neurotransmitters in the synaptic cleft, while  $\alpha$  and  $\beta$  are the forward and backward binding rates of neurotransmitters for the given receptor type. We also define the following variables:

$$\tau_r = \frac{1}{\alpha C_{\text{max}} + \beta} \quad (6)$$

$$r_{\infty} = \frac{\alpha C_{\text{max}}}{\alpha C_{\text{max}} + \beta} \quad (7)$$

where  $\tau_r$  is the time constant of channel binding,  $r_\infty$  is the steady-state fraction of open channels and  $\phi_h$  is the temperature dependent multiplier that was added to the original model.  $C_{\max}$  is the maximum concentration of transmitters. Temperature dependence was added to

this model by modifying all binding rates with the temperature multiplier  $\phi_h$ , which was also calculated according to eqn (3) above. The temperature coefficients ( $Q_{10}$ ) of AMPA and GABA<sub>A</sub> receptors were estimated based on the work of Postlethwaite *et al.* (Postlethwaite



*et al.* 2007) and Otis and Mody (Otis & Mody, 1992), respectively.

An analytical expression exists for the fraction of open receptors based on the phase of the transmitter release, which is approximated with a simple (square) pulse:

$$r = r_{\infty} + (r - r_{\infty}) \exp\left(-\frac{\varphi_h \Delta t}{\tau_r}\right) \text{ if the pulse is on} \quad (8)$$

$$r = r \exp(-\varphi_h \beta \Delta t) \text{ if the pulse is off} \quad (9)$$

For further details on the deduction of these equations refer to the original model.

Conductances were adjusted to reproduce spindle oscillation with the characteristics described by Barthó *et al.* (2014). Model cells matched the firing patterns of both TC and nRT cells, and spindles generated by the model reproduced waxing and waning behaviour but were slightly longer than the measured counterparts. Our computer codes of the model are available online at <https://github.com/BarthoLab/SpindleTemperatureModel>.

### Model topography

For the construction of the model we interpret the connections of the network as a bipartite directional graph where the two sets of nodes are the TC and nRT cells. We used a one-dimensional network: both sets of cells are on a one unit long line with equal distances between them, and the two lines of the two sets are parallel to each other. For the sake of reproducibility we used a deterministic random number generator based on the Mersenne Twister algorithm (MATLAB 2016a) to choose target cells. Our examined networks consisted of 100 TC cells and 20 nRT cells. Each TC cell targets 8 different nRT cells from the closest 20, based on a normal distribution. The nRT cells target 20 different TCs from the closest 50. We did not allow reciprocal connections in our networks. The algorithm creates the network without any consideration of the reciprocal rule, and it trims these pairs after the completion of the structure. In the case of bidirectional TC and nRT connections, one is removed based on a coin flip.

The strength of a given synaptic connection in the network is given by the weight associated with it. Connection weights are normally distributed with a mean as the default synaptic strength. This approach makes it theoretically possible to create topologically analogous networks that have completely different behaviours because of the different synapses. We created over 10,000 different networks – where the topology was based on different random seeds – and ran them for 2 s on random temperatures between 34.0 and 37.5°C.

Spindle detection methods were similar to the ones used in real life measurements. Low spindle frequency was a

sign of detection failure in most of the manually examined results, thus we automatically excluded cases with a spindle frequency lower than 8 Hz from our analysis.

### Statistical analysis

Correlations were calculated using Pearson's coefficient (MATLAB `corrcoef` function). Pooled correlation coefficients were transformed to normal distribution by the Fisher *z*-transform prior to testing, otherwise, parametric statistical tests were used based on the normality of observed distributions tested with the Kolmogorov–Smirnov test at a 0.05 significance level. In all statistical tests with no significant results, the powers of the tests were above 0.75 with the sample sizes used in the study, based on a minimal effect size of 0.2 in the case of correlation comparisons and 1 Hz for spindle frequency difference. Throughout the paper we show mean values  $\pm$  standard error of mean (SEM), unless specified otherwise. All analysis was done in MATLAB (MathWorks).

**Local heating experiments.** Spindle parameters during locally heated and control periods were compared with Student's two-sample *t* tests instead of paired *t* tests, since the number of spindles in the respective periods were different. In the case of pooled data (Fig. 2F), only those comparisons were included where the number of spindles occurring during any heating/control period was above 10. Since three comparisons were omitted based on this criterion, the Mann–Whitney test was used instead of the corresponding paired tests.

**Depth of anaesthesia.** When assessing the potential effect of body temperature on the depth of anaesthesia, we considered that the spontaneous decrease of urethane effect over time may induce spurious positive correlations with temperature in sessions where the animal was gradually heated over the time span of hours, and negative correlations during cooling sessions. Therefore, recordings within animals were broken up to heating and cooling sessions, and analysed separately. Partial correlations were calculated for three cortical LFP frequency bands (delta 1–4 Hz, beta 20–30 Hz and gamma 30–100 Hz) with temperature controlled for the effect of time using the MATLAB `partialcorr` function. Pooled correlations were tested for significance with a *t* test after the Fisher *z*-transform as described above.

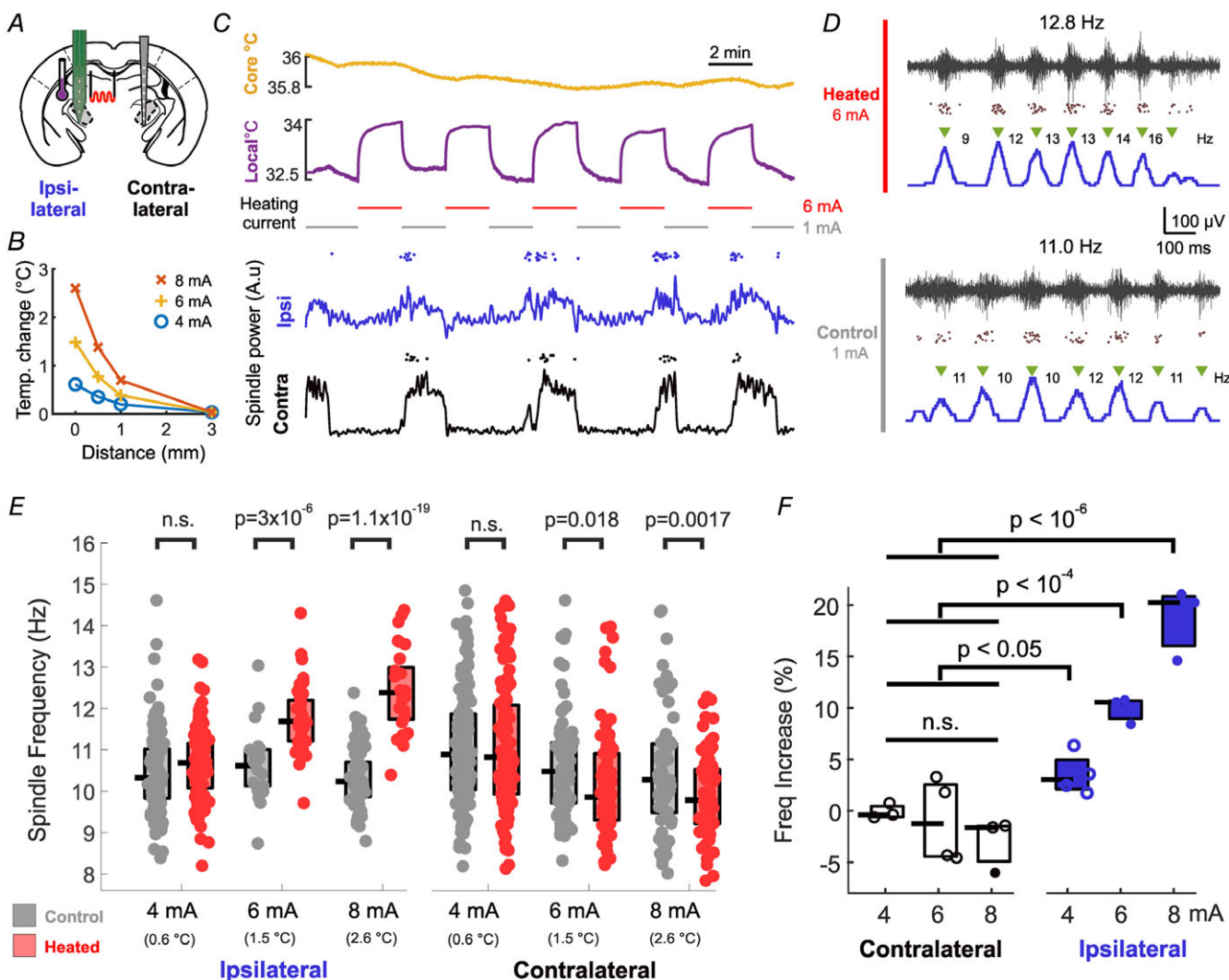
## Results

### Core and brain temperature modulate sleep spindle frequency

Our first aim was to investigate the temperature dependence of thalamocortical oscillations with no or

minimal interference from global thermoregulation. To this end we employed urethane anaesthesia, known to impair thermoregulatory processes (Malkinson *et al.* 1988), yet closely mimic natural sleep (Clement *et al.* 2008). Thus the core body temperature could be manipulated by external heating within physiological boundaries, enabling the examination of how temperature changes as large as 4–5°C alter these oscillations.

Local field potential (LFP) and multiunit activity (MUA) were recorded from the thalamus and cortex of anaesthetized mice ( $n = 8$ ) while the animals' core body temperature was varied between 34 and 39°C. To simultaneously measure brain temperature and ongoing neural activity, we used a thermoelectrode of our own design (Fekete *et al.* 2017). This probe has regular recording sites for unit activity, as well as a





temperature sensitive meander, capable of measuring the temperature of the surrounding tissue with an absolute precision of  $<0.2^{\circ}\text{C}$  (relative precision  $<0.002^{\circ}\text{C}$ ). The thermoelectrode was placed in the primary somatosensory thalamus (ventral posteromedial nucleus (VPM)/ventral posterolateral nucleus (VPL)), while 16-channel linear silicon probes were also placed in the contralateral cortex/thalamus (Fig. 1A).

We detected sleep spindles from both thalamic (VPM/VPL) and cortical MUA and calculated their frequency (Fig. 1B and C). Besides LFP and MUA signals, and brain temperature, we simultaneously recorded core temperature and electrocardiogram (see Methods) and calculated heart rate variation from the detected R-waves of the ECG signal (Fig. 1C). Figure 1D shows an example recording of core body and brain temperature under the warming and cooling protocols we used. First, after initial surgery and the implantation of sensors, by controlling the heating pad under the mouse, we let the core temperature of the animal cool down to  $35^{\circ}\text{C}$ . Next, in 30 min segments, we increased the temperature of the heating pad such that the core temperature increased by  $\sim 0.5^{\circ}\text{C}$  in each recording segment, until the core temperature reached  $39^{\circ}\text{C}$ . In half of the animals, the order of heating and cooling was interchanged. This ensured that we collected a large number of spindles in a steady state temperature of different levels, excluding the effect of temperature dynamics and directionality. Brain temperature closely followed changes in core temperature (Fig. 1D) across all animals (Fig. 1E), brain temperature being lower by  $2\text{--}3^{\circ}\text{C}$  as expected in small animals under anaesthesia (LaManna *et al.* 1989).

Spindle frequency and duration was consistently modulated by both core and brain temperature in the majority of animals, both in the thalamus and cortex. We quantified this effect by calculating the correlation between brain temperature and spindle frequency (Fig. 1F for the animal in Fig. 1D). The pooled data of correlation coefficients from all animals (Fig. 1G) where the number of detected spindles exceeded 100 (thalamus:  $n = 6$ , cortex:  $n = 7$ ) show that spindle frequency is significantly modulated by brain temperature (mean correlation coefficient ( $R$ ):  $0.37 \pm 0.18$  for thalamic,  $R: 0.34 \pm 0.3$  for cortical spindles, respectively,  $P = 0.0038$  and  $0.009$ ,  $t$  test after Fisher  $z$ -transform). Spindle duration was also significantly modulated on the pooled data (mean  $R: -0.12 \pm 0.1$ ,  $P = 0.0014$  in thalamus,  $R: -0.14 \pm 0.06$ ,  $P = 0.0019$  in cortex). These values were still statistically significant after Bonferroni correction for  $n = 4$ . On the other hand, the number of cycles per spindle and spindle prevalence showed no significant dependence on brain temperature.

To assess whether the changing body temperature influenced the depth of anaesthesia, we calculated the partial correlation of three cortical LFP frequency bands

(delta, beta and gamma) and temperature controlled for the effect of time (see Methods). Pooled partial correlation values were  $0.034 \pm 0.155$  (delta),  $0.028 \pm 0.144$  (beta) and  $0.11 \pm 0.263$  (gamma), none of which was significantly different from zero ( $t$  test after Fisher  $z$ -transform).

The modulation of spindle frequency can be expressed as the  $Q_{10}$  value (the rate of change when increasing the temperature by  $10^{\circ}\text{C}$ ) and we measured a median value of 2.44 for the thalamic spindles in our pooled data (Fig. 1H). Since in our protocol brain temperature changes followed body temperature, the examined parameters also correlated with core body temperature (Fig. 1I). In conclusion, spindle frequency increases with brain temperature, accompanied by a decrease in spindle duration, leaving the average number of spindle cycles unchanged.

### Local heating increases spindle frequency locally

Temperature dependence of sleep spindles can arise from biophysical mechanisms of the TC–nRT loop, via the direct or indirect temperature sensitivity of global modulatory systems, or a combination of both. This can be tested by locally heating the spindle-generating thalamic circuitry, with the rest of the brain and the contralateral thalamus remaining at their resting temperature. We took advantage of the fact that, besides measuring temperature, the sensor filament of our thermoelectrode is capable of heating the surrounding tissue (Fig. 2A). Passing currents at or above 4 mA, instead of the small measuring current of 1 mA, the thermoelectrode increases the local temperature in a gradual fashion up to  $3^{\circ}\text{C}$  and this heating effect is relatively local (Fig. 2B). Also, the direct current passing the probe does not stimulate the unit activity electrically (Fekete *et al.* 2017).

In these experiments, we placed the thermoelectrode with the platinum filament in the left VPM, from where we recorded both temperature as well as field and multiunit activity. The animals' core temperature was kept at  $36 \pm 0.2^{\circ}\text{C}$ . We applied heating currents of 4–8 mA. Also, we placed a linear electrode in the contralateral VPM for control recording (Fig. 2A). The heating current was applied in a cyclic protocol (2 min heating/2 min measuring), while maintaining core temperature constant (Fig. 2C). The heating cycles did not disrupt the periodic recurrence of spindling epochs, as they appeared simultaneously with those on the contralateral hemisphere (Fig. 2C bottom), and they did not disrupt the internal structure of the spindles (Fig. 2D).

As seen in Fig. 2E, application of three heating currents (4, 6, 8 mA) produced a progressive increase in local spindle frequency as compared to the control periods. The phenomenon persists in the pooled data from four animals (Fig. 2F), from a small, but significant increase of spindle

frequency at 4 mA to 20% increase at 8 mA. There was no significant increase at the contralateral thalamus, though a small spindle frequency decrease was often observable, not reaching significance in the pooled data (for statistical details, see Methods). The duration of the spindles also decreased significantly in the case of 8 mA heating by  $25.7 \pm 3.8\%$  ( $P = 0.019$ ). These results imply that the temperature dependence of spindle frequency is largely due to local biophysical mechanisms.

### **In silico TC–nRT model reproduces temperature dependence of spindle frequency**

To further elucidate the possible mechanisms of the temperature dependence of sleep spindles, we created a thalamic network model consisting of single compartment TC and nRT cells. The model consisted of 100 TC and 20 nRT cells (Fig. 3A) that were randomly connected with a loose topography and were capable of producing transient oscillations at the frequency domain of sleep spindles. Non-synaptic currents of the original Destexhe models had a built-in temperature dependency: the transition rates of the gating variables in all channel models were multiplied by a factor based on the temperature coefficient of the respective channel. The temperature coefficient had an exponential dependence on the difference between the model temperature and the experimental temperature at which the rates were measured. We used the same method to implement the temperature dependency of synaptic currents.

Figure 3B shows an example of spindles generated by the same network at 35.5 and 37°C, the latter showing a higher frequency. The pooled analysis of 500 random networks (Fig. 3C) revealed a marked correlation ( $R = 0.55$ ,  $P < 0.001$ ) between spindle frequency and temperature.

To reveal whether any single current is responsible for this effect we repeated these simulations with the temperature dependence turned on for each individual current only (TC cell  $I_T$ , nRT cell  $I_T$ ,  $I_h$ , AMPA and GABA<sub>A</sub>, respectively). We found that each current contributed to the effect by a small degree (Fig. 3D), with the exception of GABA<sub>A</sub>, which, when being temperature dependent alone, produced a small negative correlation. Thus, the model reproduced the effects of temperature change observed in mice with a statistically significant correlation between the temperature and spindle frequency as further evidence for the biophysical nature of this effect.

### **Infra-slow oscillations co-modulate temperature, heart rate and brain oscillations**

So far we have analysed the temperature dependence of thalamocortical oscillations during external manipulation. Here we were interested in the microarchitecture of brain temperature variations under natural conditions, and the effects of these changes on these oscillations.

Detailed inspection of the temperature traces under urethane revealed that besides the gross changes induced by heating and cooling, brain temperature also shows

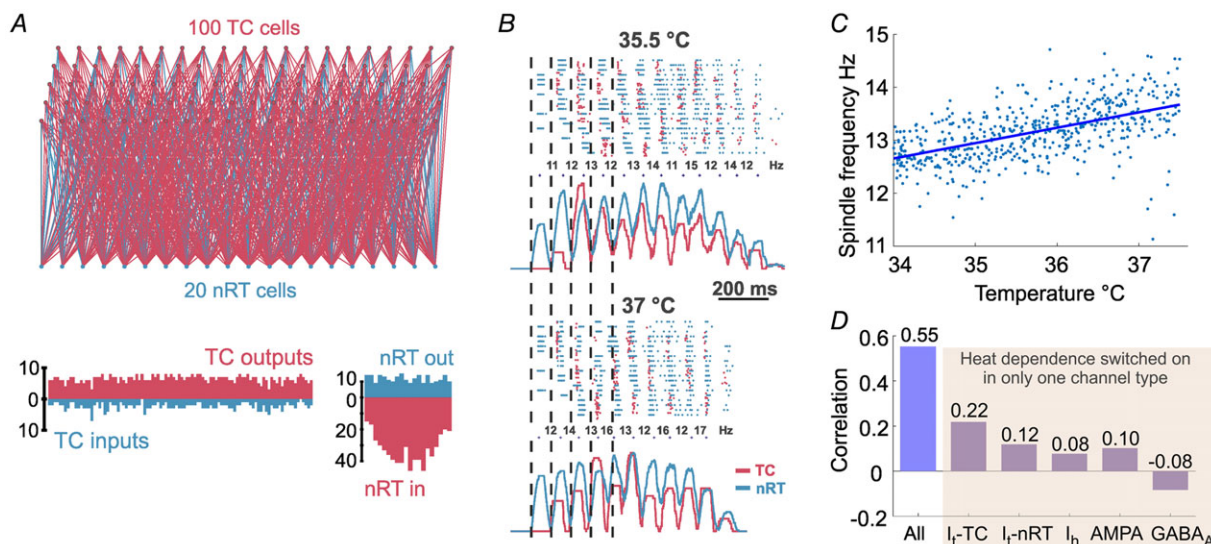


**Figure 3. Network model reproduces temperature dependence of sleep spindles**

A, schematic diagram of the network topography (above), and the number of connections for each TC and nRT cell (below). B, representative example spindles produced by the same network at two different temperatures. Top: raster plot of TC and nRT units' spiking, bottom: smoothed multiunit activity for TC and nRT cells. Note that the spindle at 37°C is faster. C, correlation between temperature and spindle frequency calculated from 500 individual spindles. D, correlations from simulations where temperature dependence was switched on for the labelled currents only. [Colour figure can be viewed at [wileyonlinelibrary.com](http://wileyonlinelibrary.com)]

periodic fluctuations on a scale smaller by an order of magnitude (Fig. 4A). These fluctuations were superimposed on, and appeared irrespectively of, the absolute brain temperature. Based on their amplitude and frequency, two types of fluctuations were differentiated. Type I fluctuations were larger ( $0.22 \pm 0.014^\circ\text{C}$  from baseline to peak) and recurred on a  $\sim 10$  min time scale (more details are provided in Table 1). Type II fluctuations were smaller ( $0.019 \pm 0.0008^\circ\text{C}$  from trough to peak), occurred with a 0.022 Hz frequency, interposed between cycles of Type I fluctuations. Under urethane anaesthesia, both types of fluctuations were associated with individual spindle events, increase in sigma power and elevation of heart rate (Fig. 4B). The periodicity of Type II fluctuations (Fig. 4C) corresponded to the frequency of infra-slow oscillation (Lecci *et al.* 2017) and there is a clear temporal order between them (Fig. 4D).

Next, we were interested in whether these temperature fluctuations also exist during natural sleep. Animals were chronically implanted with miniature negative temperature coefficient (NTC) thermistors in the thalamus (see Methods), as well as tungsten electrodes to monitor cortical and thalamic LFP and multiunit activity, electromyogram and heart rate (Fig. 5A). Both Type I and Type II fluctuations were observed in naturally sleeping animals (Fig. 5B and C).

**Table 1. Parameters of infra-slow temperature fluctuations in natural sleep and under urethane anaesthesia**

	Natural sleep	Urethane anaesthesia
No. of animals	3	3
Total recording time (h)	52.2	14.6
% of sleep	69	—
No. of sleep bouts	42	—
Mean length of sleep bout (min)	$50.65 \pm 3.6$	—
Large fluctuations (Type I)		
No. of fluctuations (fluct.)	141	19
No. of fluct. in a sleep bout	$3.92 \pm 0.3$	—
Amplitude ( $^\circ\text{C}$ )	$0.15 \pm 0.005$	$0.22 \pm 0.014$
Length (s)	$117.8 \pm 3.8$	$155.2 \pm 12.8$
Period length (s)	$639.3 \pm 36$	$963.1 \pm 119$
Small fluctuations (Type II)		
No. of fluct. epochs	133	22
Length of fluct. epochs (s)	$484.7 \pm 21.7$	$667.7 \pm 88.6$
No. of fluct. epochs in a bout	$3.69 \pm 0.4$	—
No. of fluct. cycles	1237	309
Cycle amplitude ( $^\circ\text{C}$ )	$0.012 \pm 0.0002$	$0.019 \pm 0.0008$
Cycle period length (s)	$47.9 \pm 0.5$	$44.8 \pm 1.1$
No. of cycles in an epoch	$9.1 \pm 0.5$	$14 \pm 2$

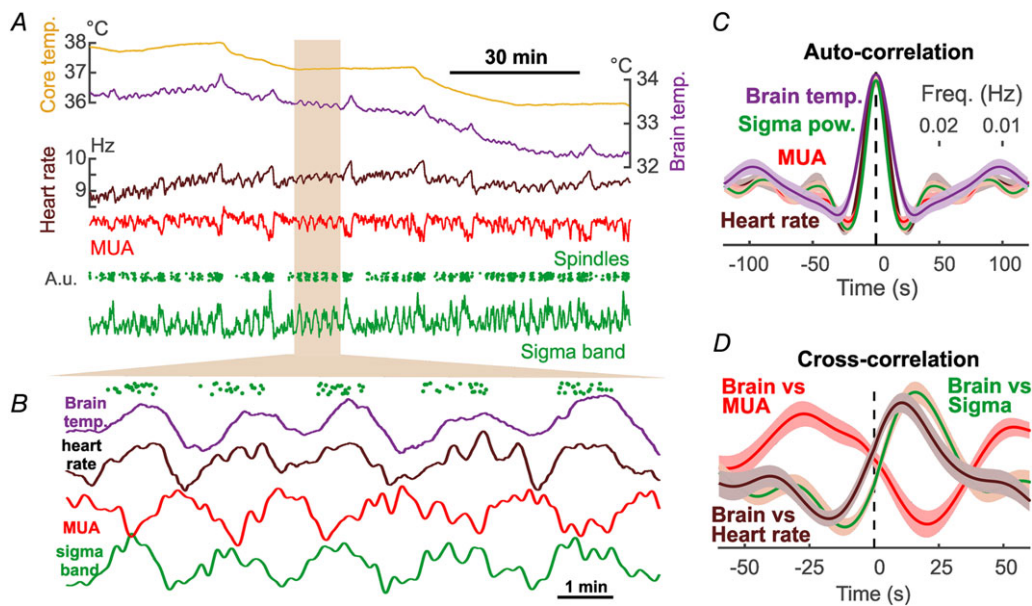


**Figure 4. Microfluctuations in brain temperature accompany spindling epochs under urethane anaesthesia**

A, example recording where microfluctuations of brain temperature, heart rate and spindle power appear to be in synchrony. B, when zooming in on a finer time scale, sigma power, heart rate and brain temperature oscillate together with an apparent temporal order between them. C, averaged autocorrelograms of pooled urethane data show that these microfluctuations are in the infra-slow frequency range ( $\sim 0.02$  Hz). D, pooled cross-correlation (brain temp vs. other) shows that spindling and heart rate foregoes brain temp fluctuation, while general multiunit activity (MUA) lags behind. Values in C and D are normalized. A.u., arbitrary units. [Colour figure can be viewed at [wileyonlinelibrary.com](http://wileyonlinelibrary.com)]

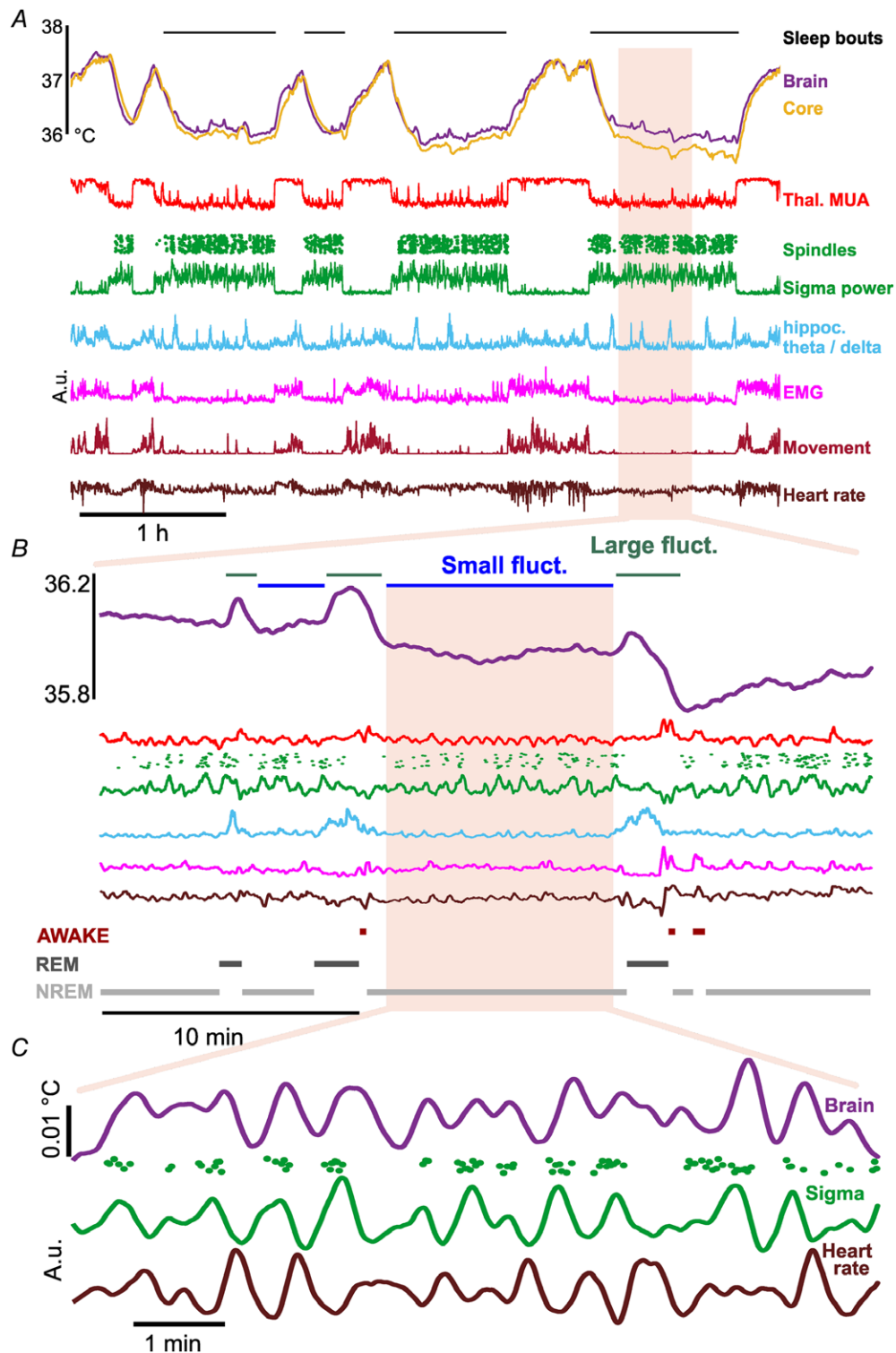


**Figure 5. Spontaneous microfluctuations of physiological signals in natural sleep**

**A**, example recording during wakefulness and sleep showing core and brain temperature, neural activity, locomotion/EMG and heart rate. Besides the brain and core temperature differences between sleep and wakefulness, smaller fluctuations are visible within sleep epochs. **B**, during a period of sleep two types of fluctuations appear in brain temperature. Large fluctuations are generally associated with increased hippocampal theta/delta ratio, while small fluctuations co-occur with sleep spindles. **C**, further zoom-in at an epoch of small fluctuations shows that brain temperature, heart rate and sigma power are co-modulated in the range of infra-slow oscillations. Except for temperature, values are in arbitrary units. [Colour figure can be viewed at [wileyonlinelibrary.com](http://wileyonlinelibrary.com)]

During natural sleep, Type I fluctuations appeared slightly more frequently than under urethane ( $0.021 \pm 0.0002$  Hz) and with a smaller amplitude ( $0.012 \pm 0.0002^\circ\text{C}$ ). They coincided with a surge in the theta/delta ratio of hippocampal activity (Fig. 5B), the hallmark of REM sleep. We analysed how changes in brain oscillations, muscle activity and heart rate correlated in time relative to the peak of these large temperature fluctuations (Fig. 6A and B shows pooled results). In general, broadband multiunit activity closely followed these elevations ( $16.5 \pm 6.6$  s median peak delay). As expected, hippocampal LFP theta/delta ratio activity was closely correlated, precluding these large temperature

fluctuations by  $8.8 \pm 5.4$  s. In contrast to urethane anaesthesia, sigma power and spindling preceded Type I elevations by a relatively large median time of  $49.4 \pm 9.6$  s. We also calculated the time lags of these parameters at half-amplitude, and these metrics confirm the temporal order described above. Averaging temperature to the onset of REM epochs confirmed that Type I fluctuations indeed accompany REM sleep (Fig. 6B). We may also see a slight increase in the averaged heart rate during these events, but this seems to be a negligible effect due to the large dispersion of the heart rate peaks relative to the respective temperature peaks. Neck muscle activity increases as both temperature as well as theta power

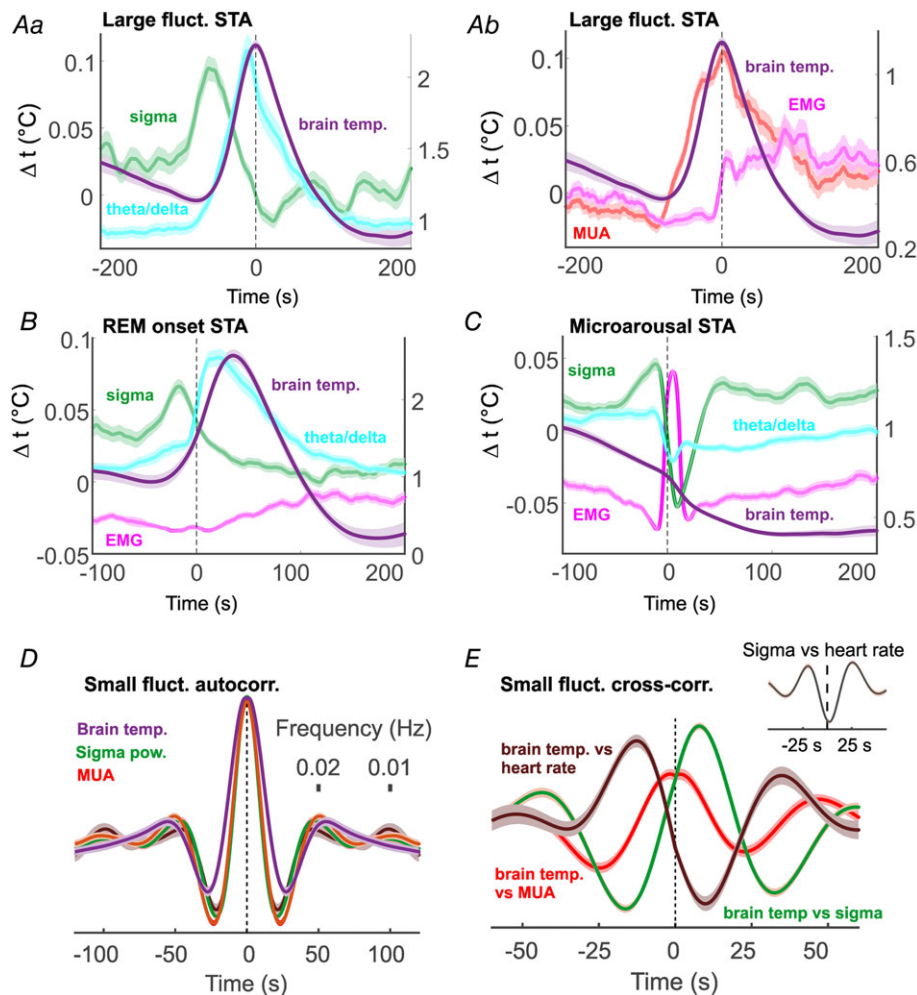


**Figure 6. Large temperature fluctuations accompany REM epochs; small fluctuations are associated with infra-slow oscillation**

Aa and b, spike triggered averages of physiological parameters relative to the peak of large fluctuations. Theta/delta ratio and thalamic multiunit activity align with temperature increase, while a sigma power and EMG decrease precedes temperature increase. B, spike triggered averages (STA) of the above parameters to REM onset. Parameters exhibit a similar pattern to that in A. C, STA triggered by microarousals. D, autocorrelogram of temperature, sigma power and MUA during small fluctuation epochs. The 0.02 Hz peak in the autocorrelogram corresponds to the frequency of the infra-slow oscillation. E, cross-correlations show that spindling foregoes temperature spikes, heart rate variation follows them, while broadband multiunit activity is in sync with the temperature. Except for temperature, values are in arbitrary units. [Colour figure can be viewed at [wileyonlinelibrary.com](http://wileyonlinelibrary.com)]

declines, which is probably due to microarousals often following REM epochs. Surprisingly, microarousals by themselves were not associated by increases in brain temperature (Fig. 6C).

Type II fluctuations under natural sleep occurred interspersed between Type I elevations, with similar parameters to those in urethane anaesthetized animals ( $0.012 \pm 0.0002^\circ\text{C}$  from trough to peak, mean period length  $47.9 \pm 0.5$  s). Their amplitude was smaller than under urethane, though this is likely to be a measurement effect, the NTC thermistor integrating signal from a larger area and therefore being less sensitive to local changes in temperature than the thermoelectrode. Type II fluctuations appeared in synchrony with thalamic multiunit activity, sigma power and individual spindles, as well as heart rate variation. Figure 6D shows the auto-correlograms of the average of all epochs, with a marked first peak in the 0.02 Hz range, corresponding to the period of infra-slow oscillation. Moreover, we found that the temporal order between these signals during these small fluctuation epochs is constrained. Broadband multiunit activity closely follows the temperature fluctuations ( $-0.65 \pm 0.8$  s delay), sigma power lags behind ( $7.5 \pm 0.8$  s delay), while heart rate variation precludes it ( $-11.92 \pm 0.9$  s delay), as the cross-correlations in Fig. 6E show. This differs from urethane data, where MUA is elevated in the opposite phase (Fig. 4D). In natural sleep, activity in VPM alternates spindling and delta epochs. Under low-dose urethane anaesthesia, however, VPM units often fire tonically between spindling epochs, with consequent higher MUA activity and temperature, despite the ongoing cortical delta activity. Note that the cross-correlation of sigma power and heart rate shows an inverse relation (Fig. 6E inset), which is in concordance with earlier results (Lecci *et al.* 2017). In summary, both REM epochs and infra-slow oscillation are accompanied by changes in brain temperature, irrespective of the baseline temperature.

## Discussion

To study the relationship of brain oscillations and temperature we recorded thalamic and cortical neural activity with simultaneous measurement of core body and brain temperature. We found that the frequency of sleep spindles correlates with brain temperature, most likely originating from the biophysical properties of local circuits, instead of the temperature sensitivity of global modulatory mechanisms. We also show that during natural sleep brain temperature is modulated by the infra-slow oscillation, as spindling and REM epochs are associated with microfluctuations in brain temperature. Our results suggest that thalamocortical oscillations and brain temperature influence each other during physiological as well as pathological states.

## Previous studies

Though temperature dependence of EEG rhythms have been described before, to our knowledge this is the first study to systematically combine LFP and multiunit recordings with brain temperature measurements, as well as use local heating and computational modelling to explain the underlying mechanism. Hoagland (1936) described higher frequency alpha-rhythms in patients undergoing hyperpyretic treatment, decreases in barbiturate-spindle frequency was found during cooling in cats (Andersen *et al.* 1967), and similar results were found in infants during surgical hypothermia (Schmitt *et al.* 2002). Also, De Vera *et al.* (1994) examined EEG activity in *Gallotia galloti* lizards and found that the frequency of spindle-like activity increases with body temperature, though these oscillations produce a continuum from 2 to 30 Hz, marking them as a different rhythm from mammalian spindles. A robust decrease in all EEG frequencies, especially theta, has been found in hibernating Djungarian hamsters (Deboer & Tobler, 1995; Deboer, 1998). Our results are generally in line with these results, as the frequency of spindle oscillations showed a positive correlation with temperature.

## Technical considerations

In the first part of this study, we used urethane anaesthesia to abolish thermoregulatory processes, so that we could manipulate the experimental animal's temperature freely. The question is, can we apply these results to unanaesthetized subjects? Urethane anaesthesia is considered a good model of natural sleep (Clement *et al.* 2008; Pagliardini *et al.* 2013), as it produces most sleep EEG rhythms with minor differences. Sleep spindles under urethane are very similar to those in natural sleep, except for their more limited spatial synchrony (Barthó *et al.* 2014). Also, as we show here, the 0.02 Hz periodic alternation between epochs of high sigma and high delta power, the so called infra-slow oscillation (Lecci *et al.* 2017), occurs both under urethane and natural sleep, with the same frequency. Finally, urethane anaesthetized animals produce REM-like epochs with characteristic hippocampal theta oscillations, though these have a lower frequency (3–5 Hz) than during real REM (6–8 Hz), and are sensitive to atropine administration (Kramis *et al.* 1975).

A seemingly surprising phenomenon in our data is that the brain temperature is consistently below the core body temperature in all anaesthetized recordings. In fact, this is a well-known phenomenon. Awake animals, and large animals under anaesthesia, have a positive brain–body temperature gradient (Hamilton, 1963; Hayward & Baker, 1969; Mitchell *et al.* 2006; Hebert *et al.* 2008). Small animals under anaesthesia, on the other hand, have

a negative brain–body temperature gradient (Serota & Gerard, 1938; McElligott & Melzack, 1967; LaManna *et al.* 1989) most likely due to the higher brain–body surface ratio, the cooling from evaporation at the craniotomy site, and the impaired thermoregulation due to the anaesthetic. Nevertheless, we show that the brain can produce spindle, theta and slow oscillations at 2–3°C below physiological brain temperature, therefore we can accept urethane anaesthesia as a suitable tool for our experiments.

### Temperature dependence of biological processes

It is well-known that temperature has an effect on the rate of biological processes (van't Hoff, 1884; Arrhenius, 1889), with a temperature coefficient ( $Q_{10}$ ) between 2 and 3, so that the speed of the process doubles or triples as temperature increases by 10°C (Demirhan *et al.* 2010). Despite a constantly redistributed cerebral heat, neuronal activity is a function of temperature; physiological and pathological temperature changes of the brain can be derived from the changes of local metabolism, cerebral blood perfusion and blood temperature (Hayward & Baker, 1969). Brain cells show a  $Q_{10}$  of 2.3 (Michenfelder & Milde, 1991) or even higher in the physiological temperature range. Temperature dependence of electrophysiological properties in the neuron is well defined. Passive membrane properties, resting potential, action potential generation, ionic transport, conduction velocity, synaptic transmission and neurotransmitter reuptake are all dependent on thermal conditions (Katz & Miledi, 1965; Brooks, 1983; Thompson *et al.* 1985; Volgushev *et al.* 2000; Tryba & Ramirez, 2004; Lee *et al.* 2005). Cerebral metabolic rate and oxygen affinity of haemoglobin are also affected by temperature change (Guyton & Hall, 2005). The sum of these effects may dramatically change neuronal network activity. Temperature dependence of neural oscillations is usually also described by the  $Q_{10}$  value, which is 2.3–2.7 for neural oscillations (Deboer & Tobler, 1995). Our results show a  $Q_{10}$  of ~2.5 in the case of sleep spindles, suggesting that this value may be a general phenomenon in the nervous system. It is worthy of note that several poikilothermic animals, such as certain crustaceans and molluscs, employ compensatory mechanisms to make their neural oscillators robust to temperature changes (Partridge & Connor, 1978; Tang *et al.* 2012). Whether a similar mechanism exists in the mammalian thalamocortical system remains to be elucidated.

### Global vs. local regulation

The main thermoregulatory centre in the brain is the preoptic area (POA) of the hypothalamus. POA receives input from peripheral thermoreceptors, but also contains intrinsically heat-sensitive neurons that are hypothesized

to monitor changes in brain temperature. The same region contains neurons that project to several modulatory centres (Peterfi *et al.* 2009) involved in sleep maintenance. POA contains warm-sensing neurons known to be activated during sleep (Alam *et al.* 1996). Therefore, it would not be surprising if body temperature influenced sleep rhythms via the posterior hypothalamus. Though it is unclear whether POA can directly influence brain thermoregulation, if it does it may influence the level of neuromodulators in the process, therefore influencing neural oscillations. Our results suggest that this is not the case, as local heating of the thalamus alters spindles ipsi- but not contralaterally. There is a possibility that locally heating the thalamus also warms the hypothalamic POA to a certain degree. Indeed, Fig. 2 shows that while local heating increases spindle frequency on the ipsilateral side, there is a smaller, non-significant adverse effect on the contralateral side that might arise from increased hypothalamic temperature perception, but this effect is smaller by a magnitude than that of local thalamic heating.

### Brain temperature changes accompany state changes

Besides brain temperature influencing neural oscillations, spontaneous changes of brain states may alter brain temperature in one way or another. We found that both REM, and on a smaller scale spindling epochs, are associated with elevated brain temperature.

Although the body's temperature regulation switches off during REM (Parmeggiani, 1977), paradoxically brain temperature increases, as has been described in rabbit (Kawamura & Sawyer, 1965), cat (Satoh, 1968), rat (Kovalzon, 1973; Obál *et al.* 1985) and even fur seal (Lyamin *et al.* 2018) (though some monkey studies reported just the opposite (Reite & Pegrarn, 1968; Hayward & Baker, 1969)). It is debated whether this effect is aimed to protect brain function from REM-associated hypothermia, or simply reflects the increased metabolic activity due to increased unit firing.

Spindling epochs in the rodent are periods resembling human stage II sleep, recurring with a periodicity of 0.02 Hz. This infra-slow oscillation has been observed in both rodents and humans (Steriade *et al.* 1993; Lecci *et al.* 2017), modulating LFP sigma band as well as heart rate (Lecci *et al.* 2017), pupil size (Blasiak *et al.* 2013) and fMRI BOLD signal (Mantini *et al.* 2007). We found that brain temperature fluctuates in synchrony with the infra-slow oscillation, including sigma power, individual spindle events, as well as heart rate. What can be the cause of these fluctuations? Physiological and pathological temperature changes of the brain can be directly derived from the changes of local metabolism, cerebral blood perfusion and blood temperature (Hayward & Baker, 1969; Wang *et al.* 2014). In our case, the temperature elevations were correlated with increased multiunit activity, which

may increase temperature directly, or via enhancing the local blood flow.

### Significance of brain rhythm alterations

What is the significance of temperature induced changes in brain rhythms? Though their exact function is still debated, the general consensus is that neural oscillations during sleep play a major role in learning and memory consolidation. Several studies reported increases in slow wave and spindle activity during sleep after learning tasks (Feld & Born, 2017). Also, transcranial DC stimulation (Marshall, 2004), or phase-locked auditory stimulation (Ngo *et al.* 2013) of slow waves during sleep can enhance consolidation of declarative memories. Aside from learning, spindle duration and frequency is affected in a variety of pathological states, including schizophrenia (Manoach *et al.* 2016). Spindle duration and frequency also correlates with intelligence (Bódizs *et al.* 2014).

As learning involves both long-term potentiation (LTP) and long-term depression (LTD) of synapses, packets of synchronized neural activity such as up-states or cycles of sleep spindles make these oscillations an ideal candidate for 'burning in' new memories. The frequency range of sleep spindles is especially suited for inducing LTP in cortical circuits (Rosanova & Ulrich, 2005). A change in the frequency of this oscillation is likely to affect synaptic potentiation in one way or another. Indeed, a 2°C drop in body temperature markedly reduces information recall (Coleshaw *et al.* 1983). Another aspect of thalamocortical oscillations is the binding hypothesis (Nikolić *et al.* 2013) stating that oscillations create a temporal window for selected groups of neurons to fire together to form a representation. Though originally proposed for gamma oscillations in awake subjects, it is probable that spindles operate along the same logic in a different scenario, in which case, frequency matters.

An alternative scenario would be that information in spindles is determined by the different groups of neurons involved in each cycle, in a synfire-chain fashion. In our data, the increase in spindle frequency was accompanied by a decrease in spindle duration, leaving the number of cycles per spindle unchanged with temperature. This would mean that the observed changes actually reflect the robustness of information encoding in spindles with regards to brain temperature.

Our data show that body along with brain temperature changes have an important but underrated role in sleep quality. Since pharmaceuticals and other medical or experimental interventions can alter brain temperature, leading to spindle frequency changes as high as 2–3 Hz, they need to be taken into consideration for the planning and analysis of both animal research and medical procedures.

### References

- Alam MN, McGinty D & Szymusiak R (1996). Preoptic/anterior hypothalamic neurons: Thermosensitivity in wakefulness and non rapid eye movement sleep. *Brain Res* **718**, 76–82.
- Alföldi P, Rubicsek G, Cserni G & Obál F (1990). Brain and core temperatures and peripheral vasomotion during sleep and wakefulness at various ambient temperatures in the rat. *Pflugers Arch* **417**, 336–341.
- Andersen P, Andersson SA & Lomo T (1967). Some factors involved in the thalamic control of spontaneous barbiturate spindles. *J Physiol* **192**, 257–281.
- Arrhenius S (1889). On the reaction velocity of the inversion of cane sugar by acids. *Zeitschrift für Physikalische Chemie* **4**, 226–248.
- Baker MA & Hayward JN (1967). Autonomic basis for the rise in brain temperature during paradoxical sleep. *Science* **157**, 1586–1588.
- Bal T, von Krosigk M & McCormick DA (1995). Role of the ferret perigeniculate nucleus in the generation of synchronized oscillations *in vitro*. *J Physiol* **483**, 665–685.
- Barthó P, Hirase H, Monconduit L, Zugaro M, Harris KD & Buzsáki G (2004). Characterization of neocortical principal cells and interneurons by network interactions and extracellular features. *J Neurophysiol* **92**, 600–608.
- Barthó P, Slézia A, Mátyás F, Faradzs-Zade L, Ulbert I, Harris KD & Acsády L (2014). Ongoing network state controls the length of sleep spindles via inhibitory activity. *Neuron* **82**, 1367–1379.
- Blasiak T, Zawadzki A & Lewandowski MH (2013). Infra-slow oscillation (ISO) of the pupil size of urethane-anaesthetised rats. *PLoS One* **8**, e62430.
- Bódizs R, Gombos F, Ujma PP & Kovács I (2014). Sleep spindling and fluid intelligence across adolescent development: sex matters. *Front Hum Neurosci* **8**, 952.
- Brooks VB (1983). Study of brain function by local, reversible cooling. *Rev Physiol Biochem Pharmacol* **95**, 1–109.
- Clement EA, Richard A, Thwaites M, Ailon J, Peters S & Dickson CT (2008). Cyclic and sleep-like spontaneous alternations of brain state under urethane anaesthesia. *PLoS One* **3**, e2004.
- Coleshaw SR, Van Someren RN, Wolff AH, Davis HM & Keatinge WR (1983). Impaired memory registration and speed of reasoning caused by low body temperature. *J Appl Physiol Respir Environ Exerc Physiol* **55**, 27–31.
- Deboer T (1998). Brain temperature dependent changes in the electroencephalogram power spectrum of humans and animals. *J Sleep Res* **7**, 254–262.
- Deboer T & Tobler I (1995). Temperature dependence of EEG frequencies during natural hypothermia. *Brain Res* **670**, 153–156.
- Delgado JM & Hanai T (1966). Intracerebral temperatures in free-moving cats. *Am J Physiol* **211**, 755–769.
- Demirhan A, Kaymaz M, Ahıska R & Güler I (2010). A survey on application of quantitative methods on analysis of brain parameters changing with temperature. *J Med Syst* **34**, 1059–1071.



- Destexhe A, Bal T, McCormick DA & Sejnowski TJ (1996). Ionic mechanisms underlying synchronized oscillations and propagating waves in a model of ferret thalamic slices. *J Neurophysiol* **76**, 2049–2070.
- Destexhe A, Contreras D, Sejnowski TJ & Steriade M (1994). A model of spindle rhythmicity in the isolated thalamic reticular nucleus. *J Neurophysiol* **72**, 803–818.
- De Vera L, González J & Rial RV (1994). Reptilian waking EEG: slow waves, spindles and evoked potentials. *Electroencephalogr Clin Neurophysiol* **90**, 298–303.
- Dijk DJ & Czeisler CA (1995). Contribution of the circadian pacemaker and the sleep homeostat to sleep propensity, sleep structure, electroencephalographic slow waves, and sleep spindle activity in humans. *J Neurosci* **15**, 3526–3538.
- Driver HS, Dijk DJ, Werth E, Biedermann K & Borbely AA (1996). Sleep and the sleep electroencephalogram across the menstrual cycle in young healthy women. *J Clin Endocrinol Metab* **81**, 728–735.
- Fekete Z, Csernai M, Kocsis K, Horváth ÁC, Pongrácz A & Barthó P (2017). Simultaneous in vivo recording of local brain temperature and electrophysiological signals with a novel neural probe. *J Neural Eng* **14**, 034001.
- Feld GB & Born J (2017). Sculpting memory during sleep: concurrent consolidation and forgetting. *Curr Opin Neurobiol* **44**, 20–27.
- Fogel SM, Smith CT & Cote KA (2007). Dissociable learning-dependent changes in REM and non-REM sleep in declarative and procedural memory systems. *Behav Brain Res* **180**, 48–61.
- Fregly MJ, Iampietro PF & Otis AB (1961). Effect of hypothyroidism on heat production and loss during acute exposure to cold. *J Appl Physiol* **16**, 127–132.
- Guyton A & Hall J (2005). *Textbook of Medical Physiology*, 11th edn. Saunders.
- Hamilton CL (1963). Hypothalamic temperature records of a monkey. *Proc Soc Exp Biol Med* **112**, 55–57.
- Hayward J & Baker M (1969). A comparative study of the role of the cerebral arterial blood in the regulation of brain temperature in five mammals. *Brain Res* **16**, 417–440.
- Hebert J, Lust A, Fuller A, Maloney SK, Mitchell D & Mitchell G (2008). Thermoregulation in pronghorn antelope (*Antilocapra americana*, Ord) in winter. *J Exp Biol* **211**, 749–756.
- Hoagland H (1936). Temperature characteristics of the “Berger rhythm” in man. *Science* **83**, 84–85.
- Katz B & Miledi R (1965). The effect of temperature on the synaptic delay at the neuromuscular junction. *J Physiol* **181**, 656–670.
- Kawamura H & Sawyer CH (1965). Elevation in brain temperature during paradoxical sleep. *Science* **150**, 912–913.
- Kiyatkin EA (2010). Brain temperature homeostasis: physiological fluctuations and pathological shifts. *Front Biosci* **15**, 73–92.
- Kiyatkin EA, Brown PL & Wise RA (2002). Brain temperature fluctuation: A reflection of functional neural activation. *Eur J Neurosci* **16**, 164–168.
- Kovalzon VM (1973). Brain temperature variations during natural sleep and arousal in white rats. *Physiol Behav* **10**, 667–670.
- Kramis R, Vanderwolf CH & Bland BH (1975). Two types of hippocampal rhythmical slow activity in both the rabbit and the rat: relations to behavior and effects of atropine, diethyl ether, urethane, and pentobarbital. *Exp Neurol* **49**, 58–85.
- LaManna JC, McCracken KA, Patil M & Prohaska OJ (1989). Stimulus-activated changes in brain tissue temperature in the anesthetized rat. *Metab Brain Dis* **4**, 225–237.
- Lecci S, Fernandez LMJ, Weber FD, Cardis R, Chatton J-Y, Born J & Lüthi A (2017). Coordinated infraslow neural and cardiac oscillations mark fragility and offline periods in mammalian sleep. *Sci Adv* **3**, e1602026.
- Lee JCF, Callaway JC & Foehring RC (2005). Effects of temperature on calcium transients and Ca<sup>2+</sup>-dependent afterhyperpolarizations in neocortical pyramidal neurons. *J Neurophysiol* **93**, 2012–2020.
- Lyamin OI, Kosenko PO, Korneva SM, Vyssotski AL, Mukhametov LM & Siegel JM (2018). Fur seals suppress REM sleep for very long periods without subsequent rebound. *Curr Biol* **28**, 2000–2005.e2.
- McElligott JG & Melzack R (1967). Localized thermal changes evoked in the brain by visual and auditory stimulation. *Exp Neurol* **17**, 293–312.
- Malkinson TJ, Cooper KE & Veale WL (1988). Physiological changes during thermoregulation and fever in urethane-anesthetized rats. *Am J Physiol Regul Integr Comp Physiol* **255**, R73–R81.
- Manoach DS, Pan JQ, Purcell SM & Stickgold R (2016). Reduced sleep spindles in schizophrenia: a treatable endophenotype that links risk genes to impaired cognition? *Biol Psychiatry* **80**, 599–608.
- Mantini D, Perrucci MG, Del Gratta C, Romani GL & Corbetta M (2007). Electrophysiological signatures of resting state networks in the human brain. *Proc Natl Acad Sci U S A* **104**, 13170–13175.
- Marshall L (2004). Transcranial direct current stimulation during sleep improves declarative memory. *J Neurosci* **24**, 9985–9992.
- Massopust LC, Wolin LR & Meder J (1965). Spontaneous electrical activity of the brain in hibernators and nonhibernators during hypothermia. *Exp Neurol* **12**, 25–32.
- Mellergård P (1995). Intracerebral temperature in neurosurgical patients: intracerebral temperature gradients and relationships to consciousness level. *Surg Neurol* **43**, 91–95.
- Michenfelder JD & Milde JH (1991). The relationship among canine brain temperature, metabolism, and function during hypothermia. *Anesthesiology* **75**, 130–136.
- Mitchell G, Fuller A, Maloney SK, Rump N & Mitchell D (2006). Guttural pouches, brain temperature and exercise in horses. *Biol Lett* **2**, 475–477.
- Morin A, Doyon J, Dostie V, Barakat M, Hadj Tahar A, Korman M, Benali H, Karni A, Ungerleider LG & Carrier J (2008). Motor sequence learning increases sleep spindles and fast frequencies in post-training sleep. *Sleep* **31**, 1149–1156.
- Ngo HVV, Martinetz T, Born J & Mölle M (2013). Auditory closed-loop stimulation of the sleep slow oscillation enhances memory. *Neuron* **78**, 545–553.

- Nikolić D, Fries P & Singer W (2013). Gamma oscillations: precise temporal coordination without a metronome. *Trends Cogn Sci* **17**, 54–55.
- Obál F, Rubicsek G, Alföldi P & Sárosi G (1985). Changes in the brain and core temperatures in relation to the various arousal states in rats in the light and dark periods of the day. *Pflugers Arch* **404**, 73–79.
- Otis TS & Mody I (1992). Modulation of decay kinetics and frequency of GABA<sub>A</sub> receptor-mediated spontaneous inhibitory postsynaptic currents in hippocampal neurons. *Neuroscience* **49**, 13–32.
- Pagliardini S, Gosgnach S & Dickson CT (2013). Spontaneous sleep-like brain state alternations and breathing characteristics in urethane anesthetized mice. *PLoS One* **8**, e70411.
- Parmeggiani PL (1977). Thermoregulation during sleep. *Riv Neurol* **47**, 485–491.
- Partridge LD & Connor JA (1978). A mechanism for minimizing temperature effects on repetitive firing frequency. *Am J Physiol* **234**, C155–C161.
- Peterfi Z, Makara GB, Obál F & Krueger JM (2009). The anterolateral projections of the medial basal hypothalamus affect sleep. *Am J Physiol Regul Integr Comp Physiol* **296**, R1228–R1238.
- Postlethwaite M, Hennig MH, Steinert JR, Graham BP & Forsythe ID (2007). Acceleration of AMPA receptor kinetics underlies temperature-dependent changes in synaptic strength at the rat calyx of Held. *J Physiol* **579**, 69–84.
- Reite ML & Pegram G V (1968). Cortical temperature during paradoxical sleep in the monkey. *Electroencephalogr Clin Neurophysiol* **25**, 36–41.
- Rosanov M & Ulrich D (2005). Pattern-specific associative long-term potentiation induced by a sleep spindle-related spike train. *J Neurosci* **25**, 9398–9405.
- Rossi S (2001). Brain temperature, body core temperature, and intracranial pressure in acute cerebral damage. *J Neurol Neurosurg Psychiatry* **71**, 448–454.
- Satoh T (1968). Brain temperature of the cat during sleep. *Arch Ital Biol* **106**, 73–82.
- Schmitt B, Jenni OG, Bauersfeld U, Schüpbach R & Schmid ER (2002). Spindle activity in children during cardiac surgery and hypothermic cardiopulmonary bypass. *J Clin Neurophysiol* **19**, 547–552.
- Serota HM & Gerard RW (1938). Localized thermal changes in the cat's brain. *J Neurophysiol* **1**, 115–124.
- Sheroziya M & Timofeev I (2015). Moderate cortical cooling eliminates thalamocortical silent states during slow oscillation. *J Neurosci* **35**, 13006–13019.
- Steriade M, McCormick DA & Sejnowski TJ (1993). Thalamocortical oscillations in the sleeping and aroused brain. *Science* **262**, 679–685.
- Sund-Levander M, Forsberg C & Wahren LK (2002). Normal oral, rectal, tympanic and axillary body temperature in adult men and women: a systematic literature review. *Scand J Caring Sci* **16**, 122–128.
- Tang LS, Taylor AL, Rinberg A & Marder E (2012). Robustness of a rhythmic circuit to short- and long-term temperature changes. *J Neurosci* **32**, 10075–10085.
- Thompson SM, Masukawa LM & Prince DA (1985). Temperature dependence of intrinsic membrane properties and synaptic potentials in hippocampal CA1 neurons in vitro. *J Neurosci* **5**, 817–824.
- Trübel HK, Sacolick LI & Hyder F (2006). Regional temperature changes in the brain during somatosensory stimulation. *J Cereb Blood Flow Metab* **26**, 68–78.
- Tryba AK & Ramirez J-M (2004). Hyperthermia modulates respiratory pacemaker bursting properties. *J Neurophysiol* **92**, 2844–2852.
- van't Hoff MJH (1884). Etudes de dynamique chimique. *Recueil des Travaux Chimiques des Pays-Bas* **3**, 333–336.
- von Krosigk M, Bal T & McCormick DA (1993). Cellular mechanisms of a synchronized oscillation in the thalamus. *Science* **261**, 361–364.
- Volgushev M, Vidyasagar TR, Chistiakova M & Eysel UT (2000). Synaptic transmission in the neocortex during reversible cooling. *Neuroscience* **98**, 9–22.
- Wang H, Wang B, Normoyle KP, Jackson K, Spitzer K, Sharrock M, Miller CM, Best C, Llano D & Du R (2014). Brain temperature and its fundamental properties: A review for clinical neuroscientists. *Front Neurosci* **8**, 1–17.
- Whitten TA, Martz LJ, Guico A, Gervais N & Dickson CT (2009). Heat synch: inter- and independence of body-temperature fluctuations and brain-state alternations in urethane-anesthetized rats. *J Neurophysiol* **102**, 1647–1656.

## Additional information

### Competing interests

None declared.

### Author contributions

P.B., M.C., S.B., K.K. contributed to the conception or design of the work, the acquisition or analysis or interpretation of data for the work and drafting the work or revising it critically for important intellectual content. D.B., Z.E., S.K. did the computational modelling. Z.F. designed and manufactured the thermoelectrode. V.B. Acquired and analyzed data. All authors have approved the final version of the manuscript and agree to be accountable for all aspects of the work. All persons designated as authors qualify for authorship, and all those who qualify for authorship are listed.

### Funding

This work was supported by the Hungarian Scientific Research Fund (OTKA K119650, PD121307), the National Brain Research Program (2017-1.2.1-NKP-2017-00002) and a Bolyai Research Scholarship of the Hungarian Academy of Sciences (P.B., B.S., Z.F.).